REGULAR ARTICLE

Preparation and Characterization of Sisal Cellulose Nanocrystals-Assembled Film

Yaqian Peng[1] · Yu Zhang[1] · Zunyan Li[1] · Helan Xu[1] · Xiuliang Hou[1]

Abstract

Cellulose nanocrystals (CNCs) extracted from sisal by acid hydrolysis were used to prepare the film with a chiral nematic phase structure by evaporation-induced self-assembly method. The effects of different acid reaction times on the morphology of sisal CNCs and the optical and mechanical properties of CNC films were investigated. Transmission electron microscopy (TEM), surface charge, and scanning electron microscopy (SEM) analysis showed that as the reaction time of acid hydrolysis increased from 30 to 90 min, the surface charge of CNCs increased from 0.116 to 0.285 mmol g^{-1} and the average length decreased from 193.6 to 100.1 nm. Sisal CNCs can self-assemble to form the film with a chiral nematic phase structure by the evaporation-inducing method. The combination of the above two aspects resulted in an increase and then a decrease in the helical pitch of CNC films. UV–Vis spectra and polarized light (POM) analysis of the CNC films revealed that the change in helical pitch can affect the color change of CNC films from blue to red and then to yellow-green. The effects of different reaction times on the nanomechanical and macroscopic mechanical properties of CNC films are reported. At the reaction time of 60 min, the macroscopic mechanical properties of the CNC film were good with a tensile strength of 43.59 MPa. This research could provide a good option for the extraction and application of sisal CNCs and create higher value-added products of sisal.

Keywords Sisal · Cellulose nanocrystals · Evaporation-induced self-assembly · Films · Optical properties · Mechanical properties

1 Introduction

Sisal is the sixth-largest fiber crop in the world, mainly in South America, Africa, and Asia. According to the Food and Agriculture Organization of the United Nations and the Chinese Bureau of Reclamation, the total global production of sisal was 206,000 tons in 2019. Brazil is the top producer in the world with more than 40% of the world's production and China ranks fourth in the world with a production of 14,000 tons in one year [1]. As compared to other plant fibers, sisal fiber has a hard texture, high strength, and higher crystallinity [2] and has good resistance to acid and alkali and high length-to-diameter ratio [3]. In China, sisal is generally used as a traditional reinforcing material to toughen sand and gravel concrete [4], polyester materials [5–7], etc.

Cellulose nanocrystals (CNCs), which are derived from natural cellulose fibers, are of increasing interest because of their excellent chemical stability and biocompatibility. CNCs are mostly prepared by extraction from cellulose materials such as cotton [8], rice straw stalks [9], sugarcane bagasse [10], and other agricultural wastes [11, 12]. The main extraction method is to degrade the amorphous zone of cellulose materials using acids [13], enzymes [14], or oxidants [15], preserving its crystalline zone [16]. CNC suspensions can form iridescent solid films with left-handed helical structures by evaporation-induced self-assembly methods [17], showing the optical properties of chiral nematic liquid crystals [18]. In CNC suspensions, the chiral nematic phase spacing of CNCs varies by size and dimensions, degree of homogeneity, surface charge (sulfur content), and ionic concentration of the medium [19]. Similarly, the helical pitch of

Yaqian Peng and Yu Zhang contributed equally to this paper and should be considered as the co-first author.

✉ Xiuliang Hou
houxl@jiangnan.edu.cn

1 Key Laboratory of Science and Technology of Eco-Textiles, Ministry of Education, Jiangnan University, 1800 Lihu Road, Wuxi 214122, Jiangsu, China

the CNC films formed by evaporation-induced self-assembly varies depending on the size and dimension, homogeneity, and hydrolysis conditions of the CNCs in the suspension. Lin [20] and Yao [19] et al. added salt and polyethylene glycol to the CNC suspension to reduce the repulsive force by shielding the surface charge and spatial effect, respectively, which led to a decrease in the helical pitch of CNC films and a blueshift of the reflected light. This can affect the film color change [21]. Honorato-Rios [22] phase-separated CNC suspensions of more uniform size by fractionation method and dried to obtain CNC films with uniform color.

Due to its high aspect ratio, high surface area, and high crystallinity [23], CNCs have an excellent reinforcement effect in nanocomposites. Adding CNC to pumpkin starch [24], polylactic acid [25], and pure polysulfone [26], respectively, as reinforcing components can increase the material modulus. Mondragon et al. found that CNCs extracted from sisal fibers had a high aspect ratio (*L/D* of 40) with a length of 403 ± 159 nm and a diameter of 10 ± 5 nm compared to flax and hemp [27]. The high aspect ratio of CNC is an ideal condition for stress transfer from the matrix to the reinforcing phase, and composites containing sisal CNCs have higher flexural strength and modulus [28]. According to the author's current knowledge, the preparation and characterization of sisal CNC films by evaporation-induced self-assembly have not been studied.

In this paper, sisal fiber was selected as the raw material for the preparation of CNCs, and 64 wt% H_2SO_4 was used to extract the nanocellulose crystals from sisal fiber. The sisal CNC film was prepared by the evaporation-induced self-assembly method. The effects of different acid reaction times on the CNC morphology and size, as well as the optical and mechanical properties of the CNC-assembled films, were mainly investigated. The study takes full advantage of

the high crystallinity of sisal fiber and the high aspect ratio of CNC to provide a new material option to improve the versatility of sisal fiber applications and create more sisal high value-added products.

2 Experimentals

2.1 Materials

The natural plant sisal fiber used for the preparation of cellulose nanocrystals was produced in Tanzania, Africa, with a density of 1.5 g cm^{-3} and a diameter of about 0.5 mm. Ethanol absolute (EtOH), methylbenzene (C_7H_8), sodium hydroxide (NaOH), sodium tetraborate decahydrate ($Na_2B_4O_7 \cdot 10H_2O$), nitric acid (HNO_3), glacial acetic acid ($C_2H_4O_2$), and sulfuric acid (H_2SO_4) were used to extract CNC from sisal fiber. The above chemicals are all purchased from Shanghai Sinopharm Chemical Reagent Co., Ltd, Shanghai, China.

2.2 Preparation of Sisal CNCs

Referring to the method studied by Li [29] and Mondragon [27], sisal fibers were used as raw materials, and sisal CNCs were extracted by pretreatment, alkali treatment, and acid hydrolysis treatment. Then the sisal CNC suspension was obtained by hydrolyzing sisal microcrystalline cellulose with sulfuric acid [30], and the preparation process is shown in Fig. 1.

Pretreatment: The sisal fiber was washed with distilled water several times and placed in the oven at 80 °C to dry for 8 h, cut into an approximate length of 4–6 mm. Under the conditions of 85 °C, the crushed sisals are placed in a 2:1
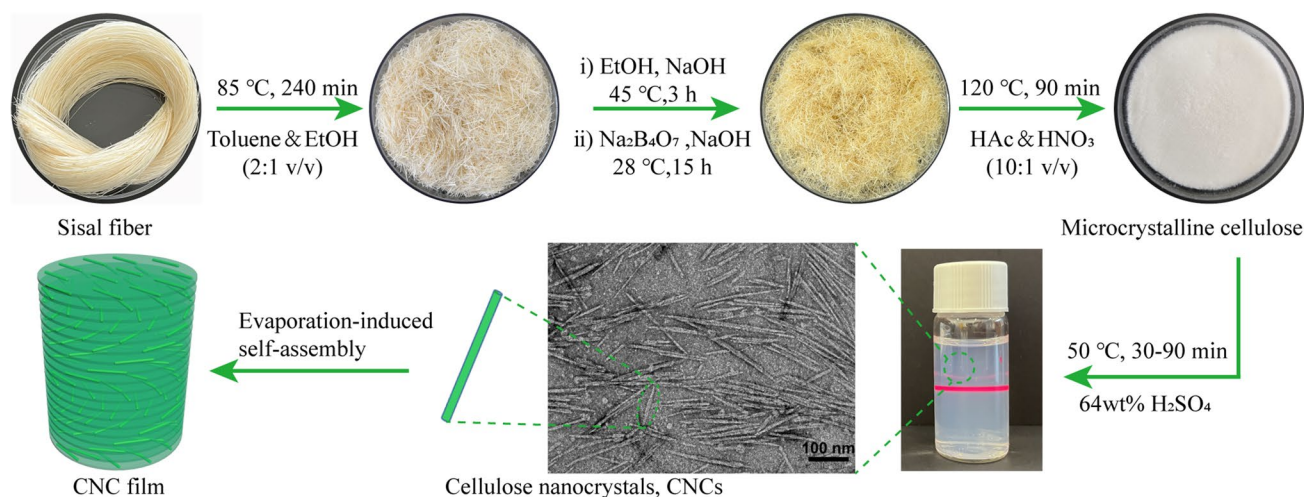

Fig. 1 Schematic representation of the extraction of sisal CNCs

volume ratio of toluene ethanol solution boiled for 240 min, ethanol washing, and drying.

Alkali and acid hydrolysis treatment: 0.2 mol NaOH was mixed with 50% ethanol solution. Sixteen grams of sisal fiber was placed in 400 ml of the mixed solution and treated at 45 °C for 3 h, washed with water, and dried. The sisal fiber was further treated with 300 ml of 10%NaOH-1%$Na_2B_4O_7 \cdot 10H_2O$ solution at 28 °C for 15 h with stirring, washed with water, and dried. The dried sample was dispersed in 300 ml of the mixed solution of 80% acetic acid and 68% nitric acid (10:1, v/v) to react for 90 min at 120 °C and washed repeatedly with ethanol and water. Finally, white sisal microcrystalline cellulose was obtained by freezing.

Preparation of sisal CNCs: 10 g of white sisal microcrystalline cellulose powder was placed into 87.5 mL of 64 wt% H_2SO_4 and slowly stirred at a constant temperature of 50 °C. The acid hydrolysis reaction was carried out at different times (30, 45, 60, and 90 min). When the reaction was finished, 900 ml of distilled water was slowly added to the beaker to dilute the acid solution. Then, the supernatant was poured off and the lower white suspension was centrifuged three times in a centrifuge (6000 r/min and 10 min), and the precipitate obtained by centrifugation was put into a dialysis membrane and dialyzed to about pH = 6. Finally, the well-dispersed CNCs suspension with Tyndall effect (concentration of 2 wt%) [31] was obtained by concentration and sonication as shown in Fig. 1.

2.3 Preparation of Sisal CNC Films

CNC films were prepared by evaporation-induced self-assembly, and CNC suspensions after four different reaction times (30, 45, 60, and 90 min) were taken out and poured into polystyrene circular molds (d = 3.5 cm). The films were made by evaporation-induced self-assembly at 20 °C and 70% RH for 72 h and labeled as CNC30, CNC45, CNC60, and CNC90.

2.4 Characterization of the Microstructures and Surface Charge of Sisal CNCs

2.4.1 Transmission Electron Microscopy Analysis (TEM)

Transmission electron microscopy (TEM) (model JEM-1400 (JEOL, Japan) was used to determine the size of CNCs in suspensions. The concentration of 1% CNC dispersion was added dropwise to the copper network for 1 min, and the floating solution was blotted off by filter paper. Then take 3 wt% phosphotungstic acid aqueous solution and add the same drop on the copper net to negatively stain the sample. The grids were dried at room temperature, and the dimensions of the imaged CNCs were tested with an accelerating voltage of 120 kV. The lengths and diameters of at least 100

CNCs samples were determined by TEM image analysis and averaged.

2.4.2 Surface Charge Analysis

Surface charge and sulfur content of CNCs were measured by the reported method [32] using CAS surface charge analyzing system (AFG ANALYTIC GMBH, Germany). One gram of 1% CNC suspension was used a standard aqueous solution and was titrated by poly (dimethyl diallyl ammonium chloride) (1–3 ml, 0.1 mol/L). The volume of titrant ($V_{titrant}$) required for the test is given according to the inflection point [32]. The sulfur content and surface charge are calculated by the following Eqs. (1) and (2), respectively.

$$\text{Sulfur content (wt\%)} = \frac{V_{titrant} C_{titrant} M_W(S)}{M_{CNC} C_{CNC}} \times 100 \tag{1}$$

$$\text{Sulface charge} \left(\text{mmol g}^{-1} \right) = \frac{V_{titrant} C_{titrant}}{M_{CNC} C_{CNC}} \tag{2}$$

where M_{CNC} and C_{CNC} are the mass and concentration of the cellulose nanocrystal suspension, respectively, and $M_W(S)$ is the atomic mass of sulfur.

2.5 Characterization of the Structure and Optical Properties of Sisal CNC Films

2.5.1 Scanning Electron Microscopy Analysis (SEM)

Scanning electron micrographs of CNC films were carried out to observe the morphology of the samples using a Sigma HD field emission electron microscope (Zeiss, Germany) at an accelerating voltage of 5 kV, with samples sputter-coated by Palladium.

2.5.2 Polarized Optical Microscopy (POM)

The texture of the CNC films was observed by placing the CNC films under mutually perpendicular polarizers in the reflection mode of the DM2700P microscope (Leica, Germany).

2.5.3 Ultraviolet–Visible Spectroscopy

The UV–Vis spectra of the CNC films over a wavelength range of 200–800 nm were recorded using the 2600 UV–Vis (Shimadzu, Japan) spectrophotometers.

2.5.4 Circular Dichroism (CD) Spectra

The CNC film samples were cut into 1.50-mm-wide strips and tested on a CD spectrometer (J-1700 spectropolarimeter (JASCO, Japan)).

2.6 Mechanical Properties of Sisal CNC Films

2.6.1 Nanoindentation Analysis

The nanoindentation experiments were performed using a TI premier nanomechanical test system (Hysitron, USA) with a Berkovich indentation tip. The experiments were calibrated beforehand using the Oliver–Pharr method [33]. During the measurement process, the indenter tip is pressed into the material by applying an increasing normal load, and partial/complete relaxation of the indenter occurs when the normal load reaches a predetermined maximum value and stays for 5 s. The maximum indentation load that can be applied to the sample is 100, 400, 700, and 1000 μN, and it can control the downward pressure and relaxation of the indenter through the actuator and sensor to provide continuous load and displacement measurement can get the load–displacement curve and obtain the real-time contact area so that the nanohardness (H) and elastic modulus (Er) can be measured.

2.6.2 Stress–Strain Measurement

The samples were cut into rectangular lengths of 30×10 mm and tested for mechanical strength at 25 °C and 30% relative humidity using a WDW-1 electronic universal testing machine (China). The loading rate was 10 mm/min, and each sample was tested at least 3 times.

3 Results and Discussion

3.1 Effect of Reaction Time on Length-Diameter Ratio and Surface Charge of Sisal CNCs

Figure 2 shows the CNC morphology in suspensions with different reaction times, and the CNCs are rod-shaped. As the reaction time increased from 30 to 90 min, the CNC rods became smaller, the length decreased from 193.6 ± 18 to 100.1 ± 20 nm, the diameter decreased from 6.5 ± 0.4 to 5.8 ± 0.3 nm, and the CNC rods and size distribution became more uniform. The results did not differ much from those of Siqueira [34] and Nancy Lis Garcia de Rodriguez [35], who reported that the sisal CNCs had lengths of 215 and 250 nm and diameters of 5 and 4 nm.

From Table 1, it can be seen that different reaction times affect the size of sisal CNCs and the surface charge. As the reaction time increased from 30 to 90 min, the sulfur content of CNCs increased from 0.37 ± 0.03 wt% to 0.91 ± 0.03 wt% and the surface charge increased from 0.116 to 0.285 mmol g^{-1}. This was mainly due to the grafting of anionic sulfate half-ester groups onto the hydroxyl site on the CNC surface by the sulfuric acid hydrolysis reaction. As the reaction time increased, the more sulfate half-ester groups were grafted onto the CNCs, the more surface charge the CNCs carried [36]. The surface charge density of CNCs was an important factor in controlling the helical pitch of

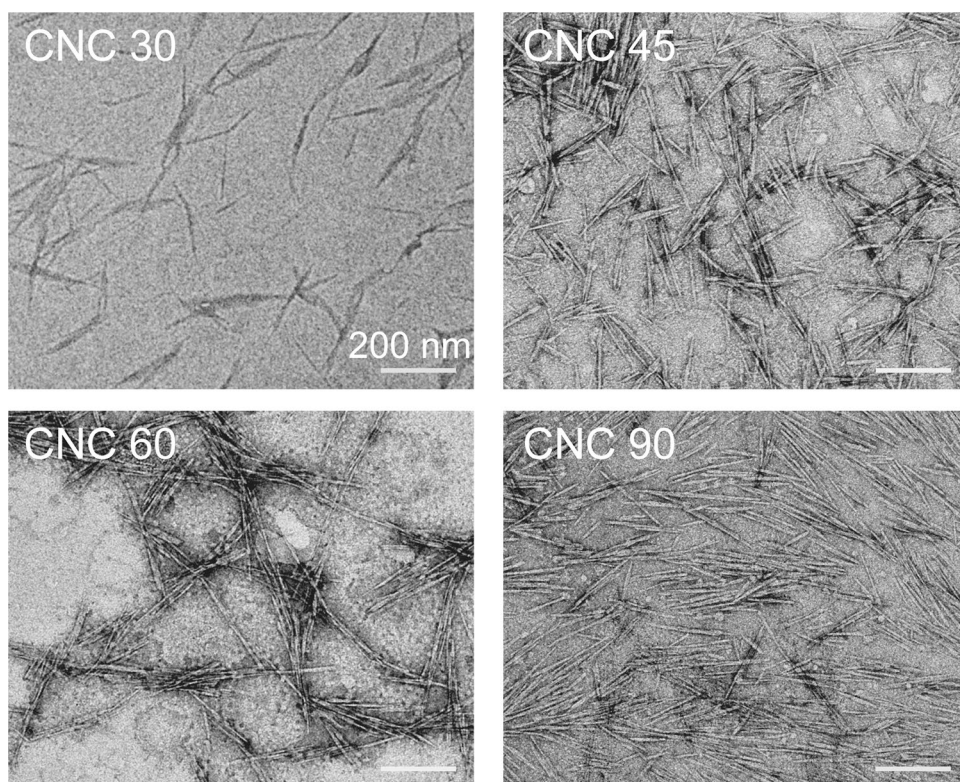**Fig. 2** TEM images of the CNCs with different reaction times

**Table 1** Effect of reaction time on the size and surface charge of sisal CNCs

Sample	Reaction time (min)	Length/L (nm)	Diameter/D (nm)	L/D	Sulfur content (wt%)	Surface charge (mmol g^{-1})
CNC30	30	193.6 ± 18	6.5 ± 0.4	30	0.37 ± 0.03	0.116
CNC45	45	167.2 ± 23	6.3 ± 0.5	27	0.63 ± 0.02	0.196
CNC60	60	143.2 ± 31	6.0 ± 0.2	24	0.70 ± 0.02	0.220
CNC90	90	100.1 ± 20	5.8 ± 0.3	17	0.91 ± 0.03	0.285

the chiral nematic structure of the CNC film [37, 38]. An increase in surface charge increased the repulsive force between CNCs, resulting in a larger helical pitch, which in turn affected the color of CNC films.

3.2 Effect of Reaction Time on the Microstructure of Sisal CNC Films

Figure 3 shows SEM images of the cross section of CNC films with different reaction times, and it can be found that the CNC films had a helical structure of chiral nematic phase. As the reaction time increased from 30 to 60 min, the helical pitch of the CNC films showed a trend of increase and increased from 329.5 to 491.2 nm measured by SEM images in Fig. 3. The dominant factor was that the surface charge becomes more and the repulsive force between CNCs becomes stronger, resulting in a larger helical pitch. The reaction time was increased from 60 to 90 min, and the helical pitch of the CNC film tended to decrease to 374 nm because the CNC size was reduced to a greater extent and the CNC distribution was more uniform. Similar results were reported for CNCs obtained from black spruce extracts by different acid reaction times [38].

Fig. 3 SEM images of the cross section of CNC films with different reaction times
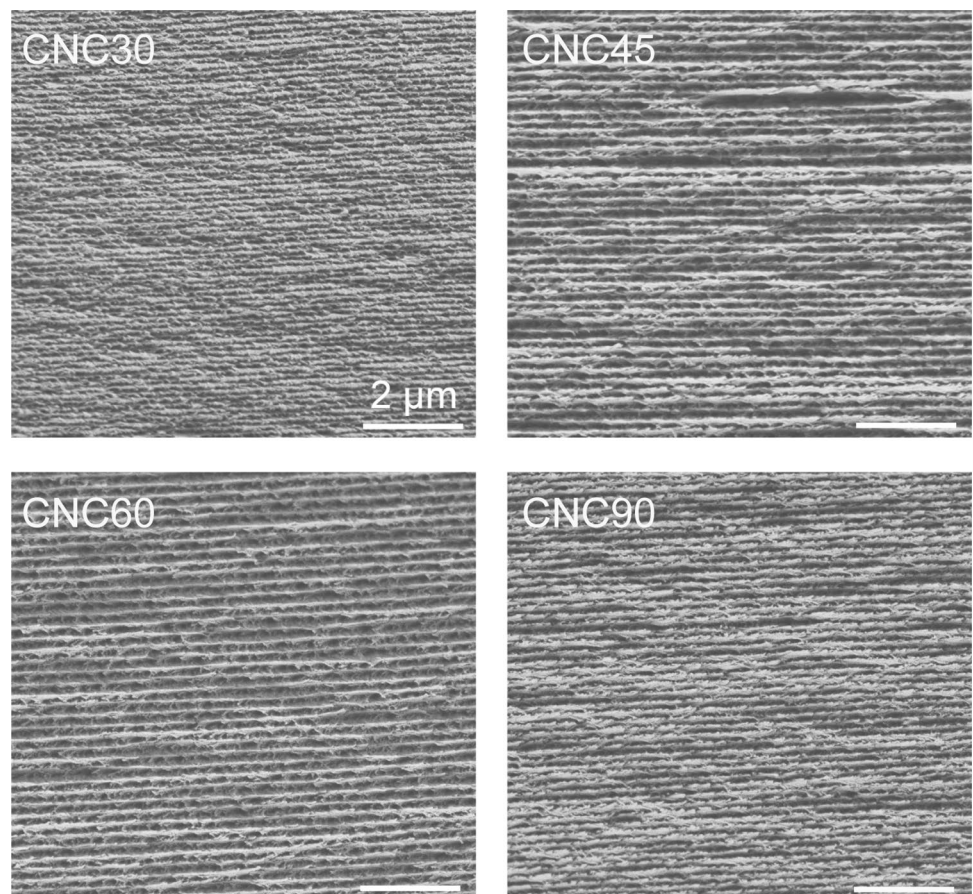
3.3 Effect of Reaction Time on Optical Properties of Sisal CNC Films

As can be seen from Fig. 4, the CNC suspension can form iridescent solid films with optical properties of chiral nematic liquid crystals after evaporation-induced self-assembly [31]. In Fig. 4b, the POM images of CNC films at different reaction times demonstrated continuous color changes and clearly showed the typical digital color texture, indicating that different reaction times did not disrupt the chiral nematic arrangement of the original CNCs. The continuous color change was also detected by both UV–Vis and CD spectra (Fig. 4c, d).

As shown in Fig. 4c, as the reaction time increased from 30 to 60 min, the absorption peak increased from 460 to 756 nm. The color of CNC films changed from blue to red, i.e., a redshift occurred. However, as the reaction time increased from 60 to 90 min, the maximum absorption peak decreased from 756 to 580 nm. The CNC films changed from red to yellow-green, i.e., a blueshift phenomenon occurred. It was mainly due to the change of the helical pitch. During the occurrence of the red shift phenomenon, the repulsive force between CNCs became larger, resulting in a larger helical pitch. But later on, because the CNC bars become smaller and more uniform, the helical pitch became smaller, so the CNC film color changed from red to yellow-green.
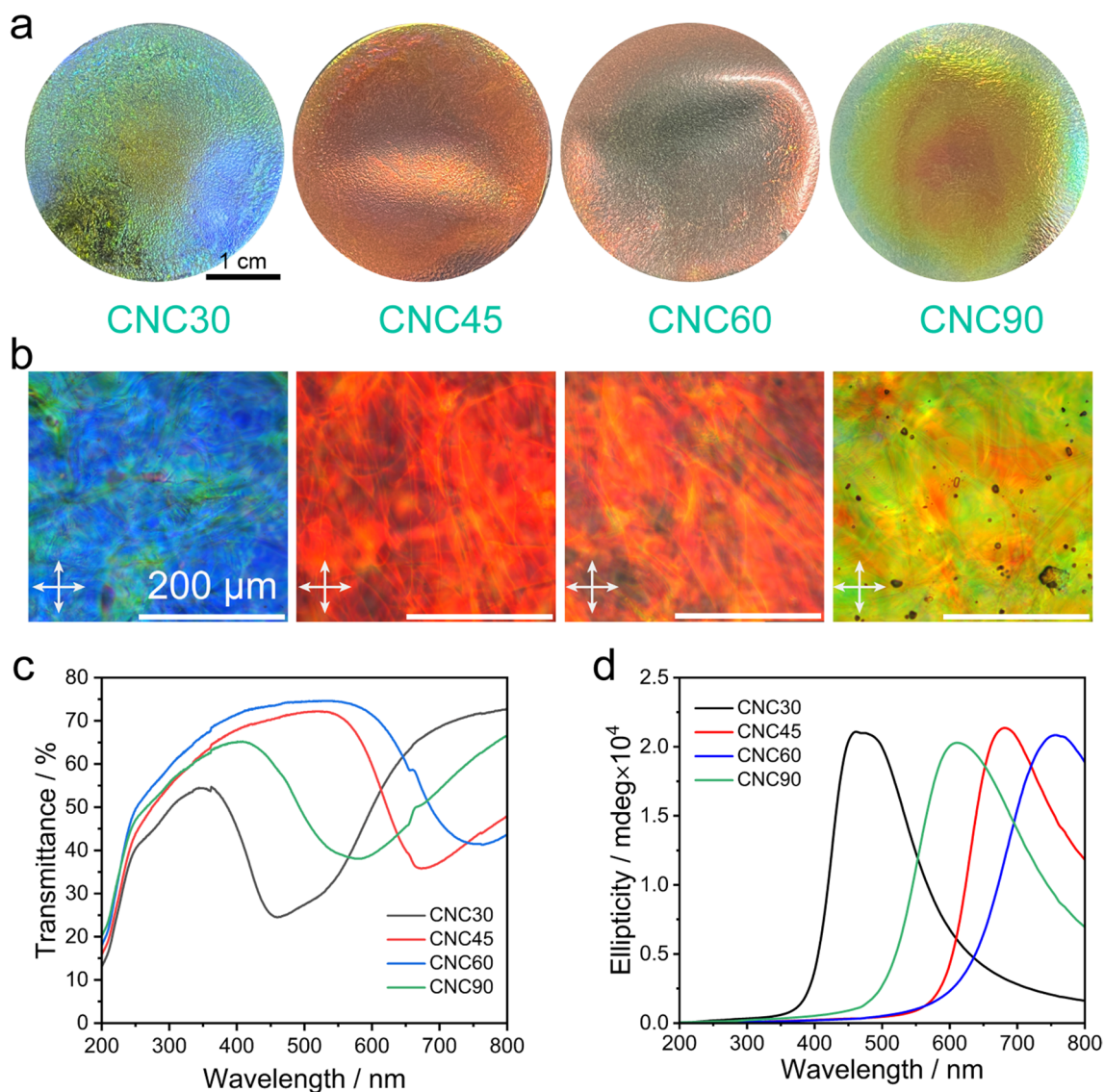

Fig. 4 Optical properties characterization of the CNC films with four different acid reaction times (CNC30, CNC45, CNC60, and CNC90); **a** actual visual color image of CNC films in natural light perpendicular to the film surface, **b** POM images of the CNC films, **c** UV–Vis spectra of the CNC films, **d** CD spectra of the CNC films

The helical arrangement of the pointing vectors in the chiral nematic structure allows the refractive index to change periodically, giving it the properties of a one-dimensional photonic crystal. When the helical pitch is a few hundred nanometers, the chiral nematic liquid crystal shows color due to the selective reflection of visible light and follows the Bragg equation:

$$\lambda_{max} = P \cdot n_{ave} \cdot \sin\theta$$

From the above equation, the maximum reflection wavelength λ_{max} is related to the helical pitch P of the chiral nematic phase structure, the average refractive index n_{ave}

of the CNC film, and the angle θ between the propagation direction of the incident light and the vertical direction of the helical axis, where λ is the center of the corresponding reflection peak ($n_{ave} = 1.5$, $\theta = 90°$). Therefore, the color change of CNC films measured in the UV–Vis spectrum (Fig. 4c) can only come from the increase of P. Moreover, the values of the helical pitch of the CNC films calculated from the UV–Vis spectra are 307, 448, 506, and 386.7 nm, which match with the measured values from the SEM photographs with little difference, as shown in Fig. 5.

Figure 6 shows that changing the angle of the CNC45 film from 0° to 80° with constant incident light, the film presents a gradual change from red to yellow-green light. This is consistent with the change in the peak presented by the UV–Vis spectrum (Fig. 6b), indicating that the CNC films had a structural color. Structural color is a type of coloration that arises from visible light interference with certain structural features at the micro- or nanoscale [39]. In recent years, structural color materials have been fabricated through a bottom-up process such as induced self-assembly. Due to its brilliant colors, it can be used as a decorative display, and in addition to that, it is also responsive and used as an anti-counterfeit or sensor. It provides more application possibilities for sisal CNC films.

3.4 Effect of Reaction Time on Mechanical Properties of Sisal CNC Films

3.4.1 Nanomechanical Properties

Figure 7 shows the characterization of the nanomechanical properties of CNC films with different reaction times. It can be found that the loading–unloading curve of the CNC film
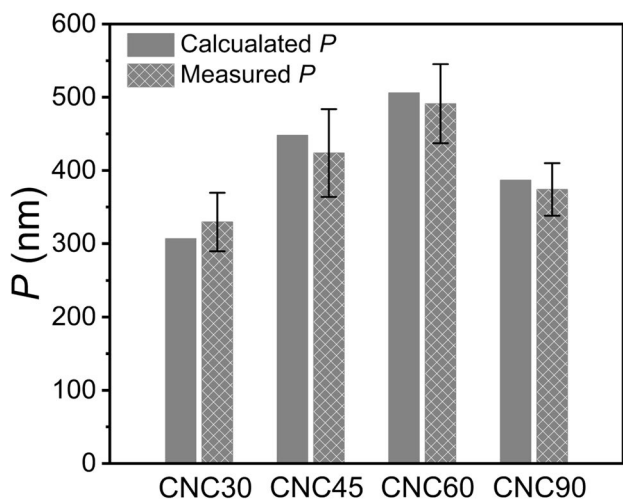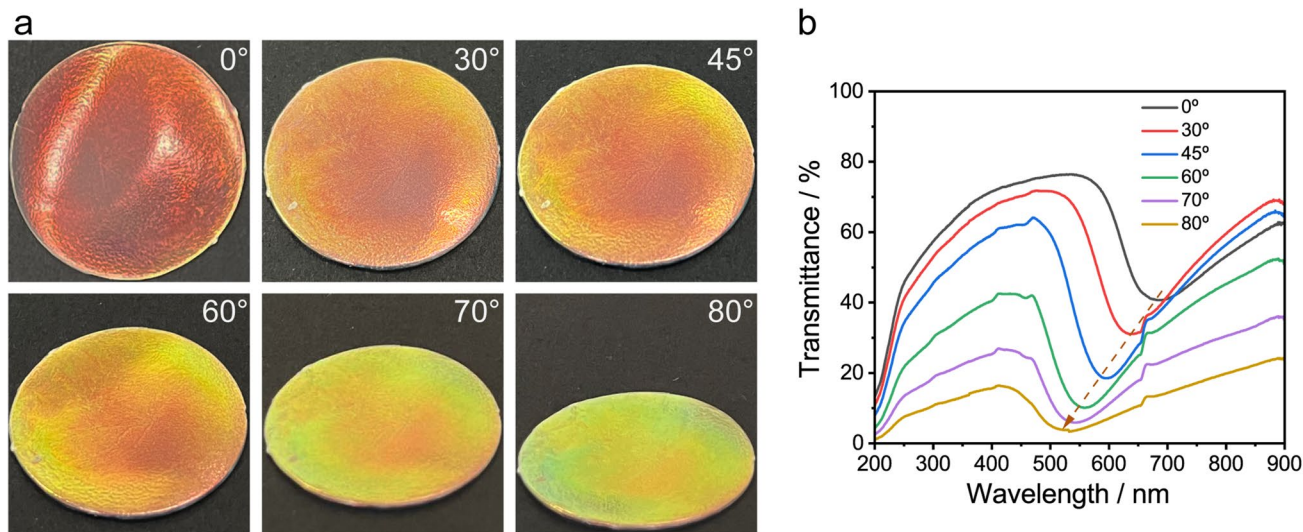
Fig. 5 Helical pitches (p) of CNC30, CNC45, CNC60, and CNC90 films were calculated from UV–Vis spectra and measured from SEM photographs, respectively

Fig. 6 **a** The photographs and **b** UV–Vis spectra of the CNC film with a reaction time of 45 min were taken at different angles
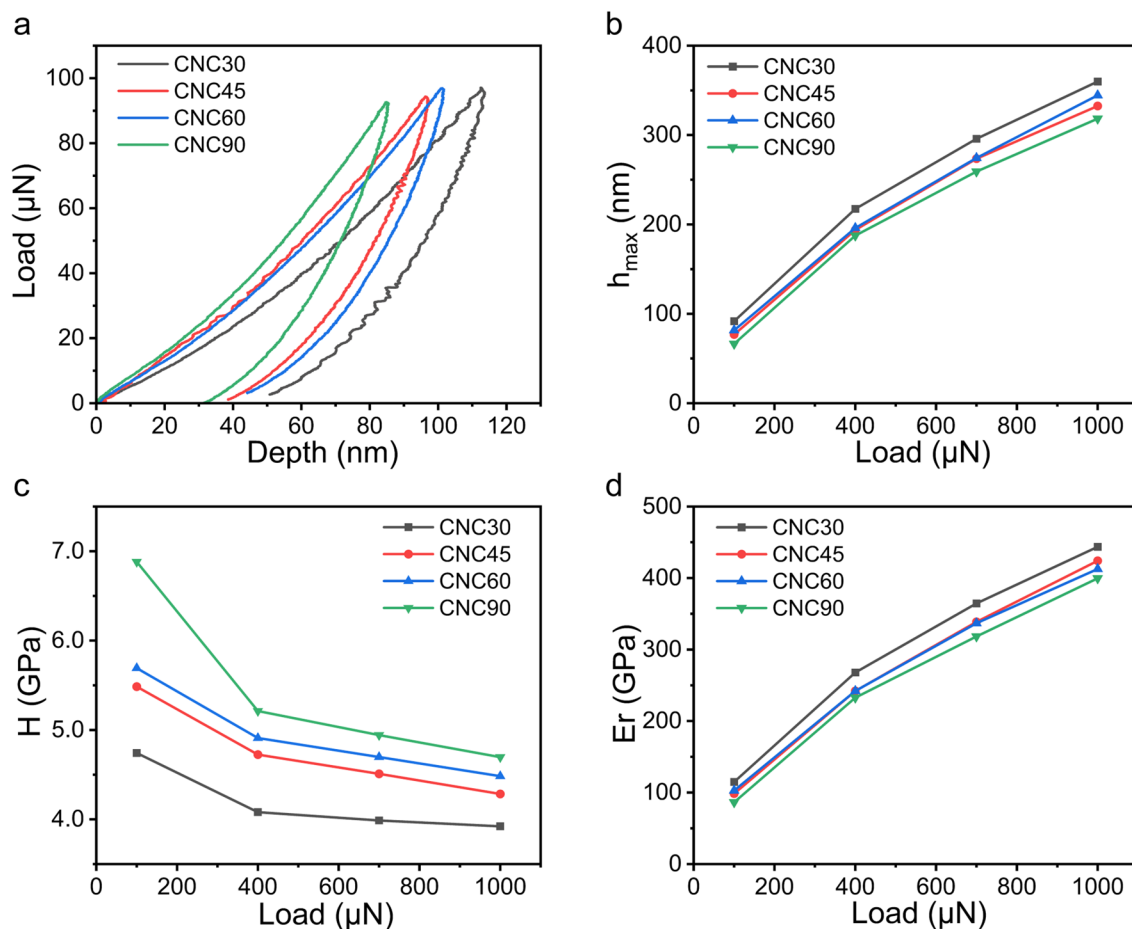
Fig. 7 a Typical load–displacement curves of CNC30, CNC45, CNC60, and CNC90 films using a maximum load of 100 µN, **b** Under different loading values (100, 400, 700, and 1000 µN), the film

loading depth relationship diagram, **c** nanohardness of the CNC films, **d** elastic modulus of the CNC films

shifts left with the increase in reaction time (Fig. 7a), which can indicate that the CNC30 film is loaded with greater indentation depth than the CNC90 film under the same force (Fig. 7b). Overall, the elastic modulus of the CNC films does not differ much, and the CNC30 film is relatively better. According to Fig. 7c, d, it can be seen that at the maximum load value of 100 µN, as the reaction time increased from 30 to 90 min, the modulus of elasticity decreases from 114.82 to 86.50 GPa and the nanohardness increased from 4.73 to 6.88 GPa. Nicolas Auclair found that the more dispersed and homogeneous the distribution of CNCs in the nanocomposites, the better their properties [40]. Thus, as the acid reaction time became longer, the CNC size became smaller and more uniformly distributed, resulting in relatively better hardness of the CNC90 film.

3.4.2 Macroscopic Mechanical Properties

Figure 8 shows the stress–strain curves of the CNC films, where the tensile stress and strain were measured at the time

of fracture. It can be seen that the four CNC films have a tensile stress of more than 32 MPa, which is higher than that of 18–25 MPa for the casted flax CNC films with glycerol as plasticiser [41]. The mechanical properties of the CNC60 film were relatively good with a highest tensile strength of 43.59 MPa, elongation at break of 0.41%, and Young's modulus of 14.9 GPa (Fig. 8b). The good mechanical properties are mainly resulted from that sisal CNCs have high crystallinity, high aspect ratio, and relatively uniform size distribution [42].

4 Conclusions

In this paper, the acid hydrolysis method was used to extract CNCs from sisal fiber and sisal CNCs could be used to prepare CNC films with chiral nematic phase structure by evaporation-induced self-assembly method. The microstructure and surface charge of sisal CNCs were characterized. It was found that as the reaction time increased from
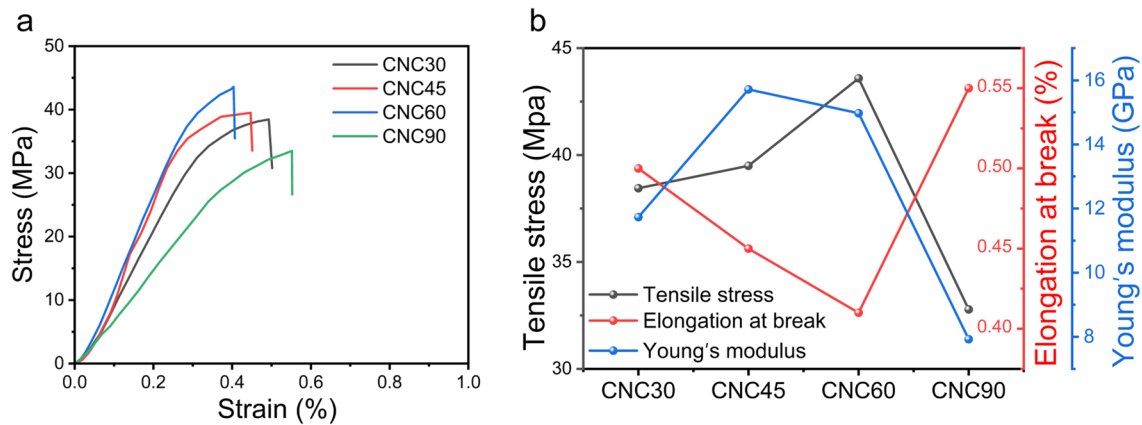
Fig. 8 Mechanical properties of the CNC films; **a** stress–strain curves of the films, **b** tensile strength, elongation at break, and Young's modulus of the CNC films

30 to 90 min, the surface charge of CNC in the suspension increased from 0.116 to 0.285 mmol g^{-1}. The size of CNC became smaller and more uniformly distributed and the average length decreased from 193.6 to 100.1 nm, the average fineness decreased from 6.7 to 5.8 nm, and the length-to-diameter ratio decreased from 30 to 17. The combination of these two factors leads to an increase in the helical pitch of the CNC film from 329.5 to 491.2 nm and then to a decrease to 374 nm.

Importantly, changes in helical pitch affect the optical properties of the CNC film. The direct response is a change in the color of the CNC film. As the reaction time increases from 30 to 60 min, the maximum absorption peak of the CNC film increased from 460 to 756 nm, and the color changed from blue to red, i.e., the redshift phenomenon occurred. And then, the reaction time increased from 60 to 90 min, the maximum absorption peak decreased from 756 to 580 nm, and the color changed from red to yellow-green, i.e., a blueshifted phenomenon occurred. It shows that the acid reaction time can control the chirality of the CNC film.

This paper reported the effects of different reaction times on the nanomechanical properties and macroscopic mechanical properties of CNC films. It was found that the macroscopic mechanical properties of the CNC film with the reaction time of 60 min were superior, with a tensile breaking strength of 43.59 MPa, elongation of 0.41%, and Young's modulus of 14.9 GPa. These results could provide a good option for the extraction and application of the sisal CNCs and create sisal higher value-added products.

Data Availability The datasets used or analyzed during the current study are available from the corresponding author on reasonable request.

Declarations

Conflict of interest The authors declare that they have no known competing financial interests or personal relationships that could have appeared to influence the work reported in this paper.

References

1. S. Juan, Z. Xin, Z. Hongyu, M. Chenyu, C. Helong, Y. Kexian, China Trop. Agric. **96**, 27 (2020)
2. R.R. Ramos Cecci, A.A. Passos, T.C. de Aguiar Neto, L.A. Silva, SN Appl. Sci. **2**, 20 (2020)
3. P. Sahu, M.K. Gupta, J. Reinf. Plast. Compos. **36**, 1759 (2017)
4. K. Ma, J. Liu, C.-H. Jiang, X.-F. Ma, L.-H. Huang, C.-Z. He, C.-Q. Qi, J. Cent. South Univ. **29**, 528 (2022)
5. V. Ilango, K. Shabaridharan, N.S. Kumar, R. Perumalraj, J. Ind. Text. **47**, 1702 (2018)
6. A.D. Gudayu, L. Steuernagel, D. Meiners, R. Gideon, J. Ind. Text. **51**, 2853S (2022)
7. T.P. Sathishkumar, J. Naveen, P. Navaneethakrishnan, S. Satheeshkumar, N. Rajini, J. Ind. Text. **47**, 429 (2017)
8. S. Elazzouzi-Hafraoui, Y. Nishiyama, J.-L. Putaux, L. Heux, F. Dubreuil, C. Rochas, Biomacromol **9**, 57 (2008)
9. P. Lu, Y.-L. Hsieh, Carbohydr. Polym. **87**, 564 (2012)
10. A. Mandal, D. Chakrabarty, Carbohydr. Polym. **86**, 1291 (2011)
11. H.A. Silverio, W.P. Flauzino Neto, N.O. Dantas, D. Pasquini, Ind. Crop. Prod. **44**, 427 (2013)
12. L. Chavez-Guerrero, M. Esneider, J. Bonilla, A. Toxqui-Teran, Fibers Polym. **21**, 66 (2020)
13. O.Y. Alothman, L.K. Kian, N. Saba, M. Jawaid, R. Khiari, Ind. Crop. Prod. **159**, 113075 (2021)
14. I.A. Sacui, R.C. Nieuwendaal, D.J. Burnett, S.J. Stranick, M. Jorfi, C. Weder, E.J. Foster, R.T. Olsson, J.W. Gilman, ACS Appl. Mater. Interfaces **6**, 6127 (2014)
15. A. Farooq, S. Jiang, A. Farooq, M.A. Naeem, A. Ahmad, L. Liu, J. Ind. Text. **51**, 664 (2021)
16. F.T. Seta, X. An, L. Liu, H. Zhang, J. Yang, W. Zhang, S. Nie, S. Yao, H. Cao, Q. Xu, Y. Bu, H. Liu, Carbohydr. Polym. **234**, 115942 (2020)
17. C. Gomri, M. Cretin, M. Semsarilar, Carbohydr. Polym. **294**, 119790 (2022)

18. B. Frka-Petesic, J.A. Kelly, G. Jacucci, G. Guidetti, G. Kamita, N.P. Crossette, W.Y. Hamad, M.J. MacLachlan, S. Vignolini, Adv. Mater. **32**, 1906889 (2020)

19. K. Yao, Q. Meng, V. Bulone, Q. Zhou, Adv. Mater. **29**, 1701323 (2017)

20. M. Lin, V.S. Raghuwanshi, C. Browne, G.P. Simon, G. Garnier, J. Colloid Interfaces Sci. **613**, 207 (2022)

21. Y. Meng, Y. Cao, H. Ji, J. Chen, Z. He, Z. Long, C. Dong, Carbohydr. Polym. **240**, 116281 (2020)

22. C. Honorato-Rios, J.P.F. Lagerwall, Commun. Mater. **1**, 69 (2020)

23. F. Kallel, F. Bettaieb, R. Khiari, A. Garcia, J. Bras, S.E. Chaabouni, Ind. Crop. Prod. **87**, 287 (2016)

24. L.Y. Zhang, J. Zhao, Y. Zhang, F. Li, X. Jiao, Q.H. Li, Int. J. Biol. Macromol. **192**, 444 (2021)

25. J.K. Pandey, C.S. Lee, S.H. Ahn, J. Appl. Poly. Sci. **115**, 2493 (2010)

26. Y. Xue, F. Han, J. Shuai, Z. Yanfang, L. Hui, Z. Bing, L. Lifang, J. Text. Res. **38**, 14 (2017)

27. G. Mondragon, S. Fernandes, A. Retegi, C. Pena, I. Algar, A. Eceiza, A. Arbelaiz, Ind. Crop. Prod. **55**, 140 (2014)

28. M. Ramesh, K. Palanikumar, K.H. Reddy, Renew. Sust. Energy Rev. **79**, 558 (2017)

29. L. Xiaojian, L. Hongxia, W. Chun, L. Jian, P. Dongming, D. Xiaodong, Polym. Mater. Sci. Eng. **28**, 160 (2012)

30. H. Kargarzadeh, I. Ahmad, I. Abdullah, A. Dufresne, S.Y. Zainudin, R.M. Sheltami, Cellulose **19**, 855 (2012)

31. Y. Zhang, Z. Tian, Y. Fu, Z. Wang, M. Qin, Z. Yuan, Carbohydr. Polym. **228**, 115387 (2020)

32. T. Abitbol, E. Kloser, D.G. Gray, Cellulose **20**, 785 (2013)

33. W.C. Oliver, G.M. Pharr, J. Mater. Res. **7**, 1564 (1992)

34. G. Siqueira, J. Bras, A. Dufresne, Biomacromol **10**, 425 (2009)

35. N.L.G. de Rodriguez, W. Thielemans, A. Dufresne, Cellulose **13**, 261 (2006)

36. S. Beck, M. Methot, J. Bouchard, Cellulose **22**, 101 (2015)

37. D.G. Gray, Nanomaterials **6**, 213 (2016)

38. S. Beck-Candanedo, M. Roman, D.G. Gray, Biomacromol **6**, 1048 (2005)

39. L. Shang, W. Zhang, K. Xu, Y. Zhao, Mater. Horiz. **6**, 945 (2019)

40. N. Auclair, A. Kaboorani, B. Riedl, V. Landry, O. Hosseinaei, S. Wang, Prog. Organ. Coat. **123**, 27 (2018)

41. E. Csiszar, S. Nagy, Carbohydr. Polym. **174**, 740749 (2017)

42. Y. Meng, Y. Cao, K. Xiong, L. Ma, W. Zhu, Z. Long, C. Dong, Membranes **11**, 242 (2021)